Journal of Marine Research, 57, 561–584, 1999

Radiative damping of near-inertial oscillations in the mixed layer

by N. J. Balmforth[1] and W. R. Young[1,2]

ABSTRACT

An idealized model of the transmission of near-inertial waves from the mixed layer into the deeper ocean is studied in order to assess the combined effects of background geostrophic vorticity and the planetary vorticity gradient. The model geostrophic flow is steady and barotropic with a streamfunction $\psi = -\Psi \cos(2\alpha y)$; the planetary vorticity gradient is modeled using the β-effect. After projection onto vertical modes, each modal amplitude satisfies a Schrödinger-like wave equation (in y and t) in which $\beta y + (\psi_{yy}/2)$ plays the role of a potential. With realistic parameter values, this potential function has a periodically spaced set of minima inclined by the β-effect.

The initial near-inertial excitation is horizontally uniform, but strong spatial modulations rapidly develop: at 20 days the near-inertial energy level is largest near the minima of the $\beta y + (\psi_{yy}/2)$ potential. Near the maxima of the $\beta y + (\psi_{yy}/2)$ potential, the mixed-layer near-inertial energy rapidly decreases, but, at these same horizontal locations, energy maxima appear immediately below the base of the mixed layer.

The β-effect and the geostrophic vorticity act in concert to produce a rapid vertical transmission of near-inertial energy and shear. Because of this radiation damping, the energy density of the *spatially averaged,* near-inertial oscillations in the mixed layer falls to about 10% of the initial level after 15 days. However, at the minima of the $\beta y + (\psi_{yy}/2)$ potential, concentrations of near-inertial energy persist in the mixed layer for at least forty days.

1. Introduction

The rate of decay of near-inertial oscillations in the mixed layer has been a focus of research since Gill (1984) noted that the very simplest theory makes the grossly unrealistic prediction that the timescale of decay is years rather than days. More recently, Balmforth, Llewellyn Smith and Young (1998) (paper I hereafter) discussed the effect of a geostrophic flow on the vertical propagation of near-inertial oscillations (NIOs) out of the mixed layer and into the deeper ocean. Paper I solved an initial-value problem in which, at $t = 0$, the mixed layer is set into horizontally uniform, slab-like motion in the zonal direction. However, in contrast to Gill's case, horizontal modulation is subsequently impressed onto this initial excitation by a pre-existing geostrophic flow, idealized as a steady barotropic

1. Scripps Institution of Oceanography, University of California at San Diego, La Jolla, California, 92093-0230, U.S.A.

2. Corresponding author *email:wryoung@ucsd.edu*

velocity field with streamfunction $\psi = -\Psi \cos(2\alpha y)$. The inverse wavenumber, α^{-1}, is the only externally imposed horizontal length scale in the problem.

The main conclusion of paper I is that the geostrophic vorticity greatly accelerates the decay of mixed-layer near-inertial activity so that there is no longer a *qualitative* difference between observed and model decay rates. However, there was a suggestion that there remains a quantitative discrepancy between model and observations: if one adjusts the model parameters Ψ and α so that the length scale and energy level of the geostrophic flow agree with observations (D'Asaro *et al.,* 1995; D'Asaro, 1995a,b) then it takes around 40 days to reduce the horizontal average of the NIO energy in the mixed layer to 10% of its initial value. This is modestly longer than the observed decay which takes 10, or at most 20 days.

There are many idealizations in the model of paper I which obscure a detailed comparison with observation. Nevertheless, in paper I it was suggested that other parameters in the model, such as the mixed-layer depth, could be further tuned to hasten the decay of mixed-layer NIOs and eliminate this discrepancy. In this paper we show that the inclusion of the β-effect (D'Asaro, 1989) provides the observed time scale, even if we continue to use the parameters of paper I. That is to say, the β-effect is a robust way of reducing the quantitative discrepancy between model and observations without fine tuning of poorly constrained parameters such as the mixed-layer depth.

The result of the β-effect alone (without geostrophic vorticity) was investigated by D'Asaro (1989) who showed that the β-effect results in a gradual change in the north-south wavenumber of NIOs. This 'β-shift' results in a dephasing of the different vertical modes which constitute the initial excitation and so there is vertical propagation. We show that the β-shift acts in concert with the background geostrophic flow in accelerating the downward propagation of NIOs. The result is a rapid decay of the horizontal average of the mixed-layer near-inertial energy, so that there is no longer any quantitative discrepancy between model and observations. This rapid decay requires *both* geostrophic flow and the β-effect; the two processes together are more effective than either acting alone. Thus, while we do not dispute the obvious point that a sinusoidal shear flow is an unrealistic representation of the geostrophic turbulence in the ocean, our main conclusion is that this simple model can easily match the time scale observed in ocean data.

2. Formulation of a tractable problem

a. The NIO approximation

As in paper I, our point of departure is the NIO approximation of Young and Ben Jelloul (1997). This approximation is an asymptotic expansion based on the assumption that $|\omega - f_0| \ll f_0$, where ω is the wave frequency and f_0 is the local inertial frequency. The approximation represents the NIO velocity field, (u, v, w), buoyancy, b, and pressure, p, in

terms of a single complex field, $\mathscr{A}(x, y, z, t)$:

$$\begin{aligned} u + \mathrm{i}v &= e^{-\mathrm{i}f_0 t} L\mathscr{A}, \\ w &= -\frac{1}{2} f_0^2 N^{-2} (\mathscr{A}_{zx} - \mathrm{i}\mathscr{A}_{yz}) e^{-\mathrm{i}f_0 t} + c.c., \\ b &= \frac{\mathrm{i}}{2} f_0 (\mathscr{A}_{zx} - \mathrm{i}\mathscr{A}_{yz}) e^{-\mathrm{i}f_0 t} + c.c., \\ p &= \frac{\mathrm{i}}{2} f_0 (\mathscr{A}_x - i\mathscr{A}_y) e^{-\mathrm{i}f_0 t} + c.c., \end{aligned} \tag{2.1a–d}$$

where L is a differential operator defined by

$$L\mathscr{A} \equiv (f_0^2 N^{-2} \mathscr{A}_z)_z, \tag{2.2}$$

and $N(z)$ is the buoyancy frequency.[3] For a physical interpretation, notice that $L\mathscr{A}$ provides the back-rotated, horizontal velocity field.

For a background, barotropic, geostrophic flow, $\mathscr{A}$ evolves according to the equation,

$$L\mathscr{A}_t + \frac{\partial(\psi, L\mathscr{A})}{\partial(x, y)} + \frac{\mathrm{i}}{2} f_0 \nabla^2 \mathscr{A} + \mathrm{i}\left(\beta y + \frac{1}{2}\zeta\right) L\mathscr{A} = 0, \tag{2.3}$$

where $\psi(x, y)$ is the steady, barotropic streamfunction, $\zeta \equiv \nabla^2\psi$ is the corresponding vorticity and ∇^2 is the horizontal Laplacian, $\nabla^2 = \partial_x^2 + \partial_y^2$. Eq. (2.3) is solved subject to the boundary condition that w vanishes on the boundaries, which translates to $\mathscr{A}_z = 0$ at the top and bottom of the ocean.

The asymptotic expansion inherent in the reduction of the linearized primitive equations to (2.3) is based on the assumption that the wave frequencies are close to f_0. That is, it is a multiple timescale approximation intrinsic to NIOs, and makes no assumption of separation between the horizontal length scales of the NIOs and the background geostrophic flow.

b. Projection onto vertical normal modes

In Gill's (1984) notation, the Sturm-Liouville problem associated with the linear operator L in (2.2) is

$$\frac{\mathrm{d}\hat{p}_n}{\mathrm{d}z} = -N^2 \hat{h}_n, \qquad c_n^2 \frac{\mathrm{d}\hat{h}_n}{\mathrm{d}z} = \hat{p}_n, \qquad \Rightarrow \qquad L\hat{p}_n + R_n^{-2}\hat{p}_n = 0, \tag{2.4a,b,c}$$

where c_n is the 'speed' of mode n and $R_n = c_n/f_0$ is the modal Rossby radius. The boundary

3. In paper I, Eq. (2.2) is incorrect; this is corrected in the current (2.2) above.

conditions are that $\hat{h}_n = d\hat{p}_n/dz = 0$ at $z = 0$ and $z = -H$. The eigenmodes are orthogonal:

$$\int_{-H}^{0} \hat{p}_n(z)\hat{p}_m(z)\,dz = (H_{mix}/\sigma_n)\delta_{mn}, \qquad \int_{-H}^{0} N^2(z)\hat{h}_n(z)\hat{h}_m(z)\,dz = (H_{mix}/c_n^2\sigma_n)\delta_{mn}, \quad (2.5a,b)$$

where σ_n is a normalization constant and δ_{mn} is the Kronecker delta.

We use (2.5) to project $\mathscr{A}$ onto the basis set in (2.4):

$$\mathscr{A}(x, y, z, t) = \sum_{n=1}^{\infty} \mathscr{A}_n(x, y, t)\hat{p}_n(z). \quad (2.6)$$

Each modal amplitude then satisfies the Schrödinger-like equation,

$$\frac{\partial \mathscr{A}_n}{\partial t} + \frac{\partial(\psi, \mathscr{A}_n)}{\partial(x, y)} + i\left(\beta y + \frac{1}{2}\zeta\right)\mathscr{A}_n = \frac{i\hbar_n}{2}\nabla^2\mathscr{A}_n, \quad (2.7a)$$

where

$$\hbar_n \equiv f_0 R_n^2 \quad (2.7b)$$

is the 'dispersivity' of mode n.

c. Equations for zonal geostrophic flow

In this paper, we confine attention to problems in which there is no dependence on the zonal coordinate. Thus the Jacobian in (2.7a) is zero and we can rewrite the equation in the form:

$$i\hbar_n \mathscr{A}_{nt} = -\frac{\hbar_n^2}{2}\mathscr{A}_{nyy} + V_n\mathscr{A}_n, \quad (2.8a)$$

where

$$V_n \equiv \hbar_n[\beta y + \tfrac{1}{2}\zeta]. \quad (2.8b)$$

Eq. (2.8) is the same as Schrödinger's equation for the motion of a particle (with mass $m = 1$) in a potential V_n. It is amusing that the analog of Planck's constant, $\hbar_n$, is a strong function of the vertical mode number n. Moreover, as $n \to \infty$, the Sturm-Liouville problem in (2.4) and (2.5) indicates that $\hbar_n \propto n^{-2}$. Thus, as the vertical mode number n increases we approach the classical limit. This is also the limit in which the short-wavelength approximation and ray tracing are valid (Kunze, 1985).

If $\zeta = 0$, then (2.8) is equivalent to the motion of a particle falling in a gravitational potential, $V_n = \hbar_n\beta y$. Thus, "particles" (i.e., near-inertial wave packets) accelerate toward the equator with constant acceleration, $g_n = \beta\hbar_n$. Furthermore, wave packets of different vertical order n accelerate at different rates leading to a dephasing of the initial condition, and therefore downward radiation of the energy. This is the interpretation of D'Asaro's β-dispersion mechanism in the quantum analogy.

For an $n = 1$ mode with a radius of deformation $R_1 = 20$ km, and $f_0 = 10^{-4}$ s^{-1}, one has

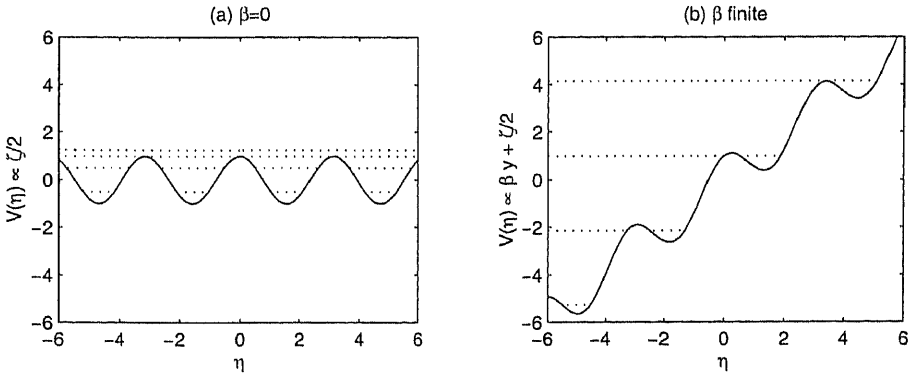

Figure 1. The potential $V_n(y) \propto \beta y + (\zeta/2)$ in (2.10). (a) $\hat{\beta} = 0$; the dotted lines schematically indicate the eigenfrequencies (equivalently, energy levels) of some of the eigenmodes described by paper I. The mode with negative eigenfrequency is 'subinertial.' (b) $\hat{\beta} = 0.96$. In this case there are no true modes. Instead there are disturbances which, for a time, remain trapped in the local minima of the laddered potential. However, these disturbances eventually tunnel through the potential barrier and fall toward the equator (see Fig. 4). In (b) the dotted lines indicate the eigenfrequencies of these 'leaky modes.'

$\hbar_1 = 4 \times 10^4\ \mathrm{m^2\ s^{-1}}$. On taking $\beta = 10^{-11}\ \mathrm{m^{-1}\ s^{-1}}$, we find that the effective gravity for the gravest vertical mode is $g_1 = 4 \times 10^{-7}\ \mathrm{m\ s^{-2}}$. Thus, in 12 days ($10^6$ seconds), an $n = 1$ 'particle' starting from rest will have "fallen' 200 km. However, as the mode number increases, the 'gravity' is weaker. For instance, a typical Rossby radius for a $n = 5$ mode is $R_5 = 5$ km so that $g_5 = g_1/16$. Thus the β-shift mechanism is most effective for low vertical modes.

To assess the effect of the background geostrophic flow, we adopt the sinusoidal shear flow of paper I:

$$\psi = -\Psi \cos 2\alpha y, \qquad \zeta = 4\alpha^2 \Psi \cos 2\alpha y. \tag{2.9a,b}$$

The potential in (2.8b) can be written as

$$V_n = 2\hbar_n \alpha^2 \Psi(\hat{\beta}\eta + \cos 2\eta), \tag{2.10}$$

where

$$\eta \equiv \alpha y, \qquad \text{and} \qquad \hat{\beta} \equiv \frac{\beta}{2\alpha^3 \Psi}. \tag{2.11a,b}$$

The nondimensional β-parameter in (2.11), $\hat{\beta}$, is the ratio of the dimensional planetary vorticity gradient, β, to a typical gradient of the geostrophic vorticity, $\alpha^3\Psi$.

The potential (2.10) is illustrated in Figure 1. When $\hat{\beta} < 2$, the potential has a regularly spaced set of minima (see Fig. 1b), but these are "inclined" by the β-effect. In quantum mechanics a potential such as that in Figure 1b is known as a 'Wannier-Stark ladder.' From

Table 1. Numerical values of the parameters for the 'standard case.' The nondimensional planetary vorticity gradient defined in (2.11) is $\hat{\beta} = 0.96$.

Quantity	Symbol	Typical numerical value
Ocean depth	H	4200 m
Mixed layer depth	H_{mix}	50 m
Stratification parameter	s	2.5 m s^{-1}
Vertical scale of N	z_0	4329.6 m
N at base of mixed layer	N_{mix}	0.01392 s^{-1}
Inertial frequency	f_0	10^{-4} s^{-1}
Length scale of geostrophic flow	α^{-1}	80,000 m
Maximum geostrophic streamfunction	Ψ	4000 m^2 s^{-1}
Minimum geostrophic vorticity	$\zeta_{min} = -4\alpha^2\Psi$	-2.5×10^{-6} s^{-1}
Kinetic energy density	$K = (\alpha\Psi)^2$	$1/400$ m^2 s^{-2}
Time scale	$T = 2/\lvert\zeta_{min}\rvert$	9.26 days
Planetary vorticity gradient	β	1.5×10^{-11} m^{-1} s^{-1}

the oceanographic perspective, the physical mechanism is clear and potentially important to the latitudinal propagation of NIOs: without β, near-inertial waves are trapped in regions of negative geostrophic vorticity. If $\beta \neq 0$, sufficiently deep negative vorticity wells will continue to trap wave packets and impede their fall to the equator. But the trapping only delays and does not prevent the fall: an initially trapped wavepacket will eventually 'tunnel' through the potential barrier and escape equatorward.

d. The model buoyancy profile and the initial condition

Following paper I, we use the model buoyancy profile introduced by Gill:

$$N(z) = \begin{cases} 0, & \text{if } -H_{mix} < z < 0; \\ s/(z_0 - H - z), & \text{if } -H < z < -H_{mix}. \end{cases} \tag{2.12}$$

(Gill placed $z = 0$ at the bottom of the ocean; we prefer to use the convention that $z = 0$ is the surface of the ocean.) Typical values for the parameters are given in Table 1. Gill (1984) solves (2.4) with $N(z)$ in (2.12) and gives simple analytical expressions for the eigenfunctions $\hat{p}_n$ and $\hat{h}_n$ and the normalization constant, σ_n in (2.5). Additional details of these normal modes are given in paper I and in Zervakis and Levine (1995).

In this paper we use the initial condition from paper I. Specifically, we take

$$u_I(z) \equiv \sum_{n=1}^{40} \epsilon_n \sigma_n \hat{p}_n(z), \qquad \epsilon_n \equiv \mathcal{N} \exp(-n^2/600), \tag{2.13a,b}$$

and $v_I(z) = 0$. The factor, $\mathcal{N}$ in (2.13b), is computed to ensure that $u_I(0) = 1$ ($\mathcal{N} \approx 1.20$). The function $u_I(z)$ is constant within the mixed layer and decreases rapidly, but smoothly, to zero below the mixed layer (see Fig. 2); $u_I(z)$ is a smoothed and continuous version of Gill's (1984) initial condition in which the mixed layer is set into impulsive motion as a slab. This ensures that the initial shear is finite (though discontinuous, see Fig. 2).

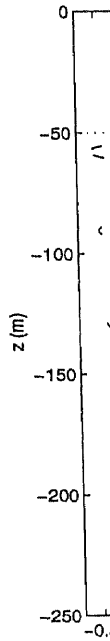

Figure 2. The
eigenfunctio
initial shear
immediately

In paper I,
employ only
numerically s
$\beta = 0$) empl
generous vert
numerical sol
between 40
energy, but th
do not alter o

We projec
vertical norm

Thus, the pro

subject to (2

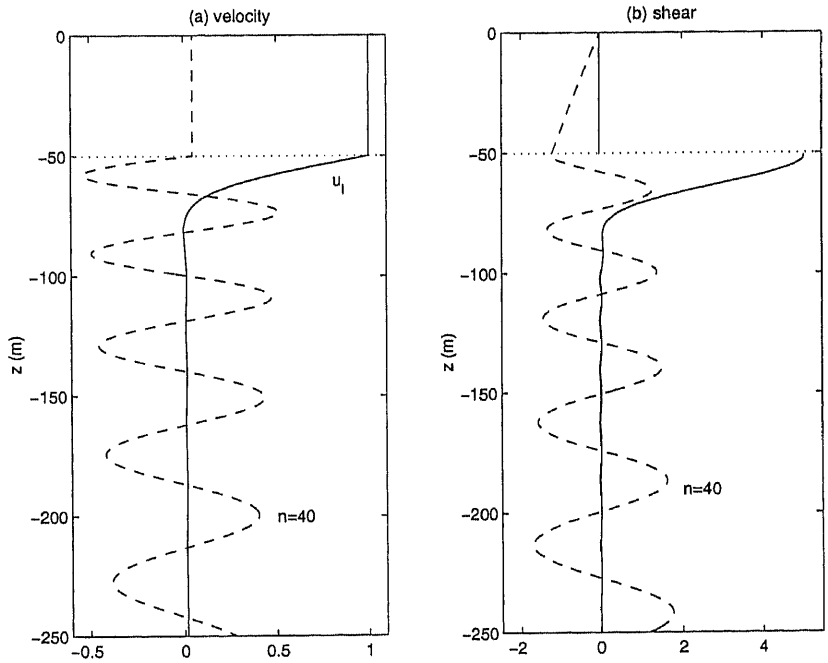

Figure 2. The initial condition in (2.13). Panel (a) shows the initial velocity $u_I(z)$ and the eigenfunction $\hat{p}_{40}(z)$ of the highest-order vertical mode used in the truncation. Panel (b) shows the initial shear and the eigenfunction $\hat{h}_{40}(z)$. The maximum value of the initial shear, which occurs immediately below the base of the mixed layer at $z = -51$ m, is $u_z \approx 5.057$.

In paper I, 80 vertical modes were used in the modal decomposition; in (2.13) we employ only 40. As a practical matter we use only 40 vertical modes because we must numerically solve (2.8) by time stepping for each vertical mode ($n = 1$ to 40). Paper I (with $\beta = 0$) employed an analytic solution involving Mathieu functions and so obtained generous vertical resolution at a modest computational expense. Comparison of our $\beta = 0$ numerical solutions with the equivalent solutions from paper I shows that the difference between 40 and 80 vertical modes is insignificant for the evolution of the near-inertial energy, but there are some slight differences in the shear. However, the differences in shear do not alter our qualitative conclusions.

We project the initial condition, $L\mathscr{A}(y, z, 0) = u_I(z)$ in (2.13), onto the basis set of vertical normal modes as follows:

$$\mathscr{A}_n(y, 0) = -R_n^2 \epsilon_n \sigma_n. \tag{2.14}$$

Thus, the problem is to solve

$$\mathscr{A}_{nt} + \mathrm{i}[\beta y + 2\alpha^2 \Psi \cos(2\alpha y)]\mathscr{A}_n = \frac{\mathrm{i}\hbar_n}{2}\mathscr{A}_{nyy}, \tag{2.15}$$

subject to (2.14).

e. Changing frame

There is a transformation of (2.15) which greatly simplifies the ultimate numerical solution; define $\tilde{\mathcal{A}}_n$ by

$$\mathcal{A}_n(y, t) = \exp\left[-i\beta yt - \frac{i\hbar_n}{6}\beta^2 t^3\right]\tilde{\mathcal{A}}_n(y, t). \tag{2.16}$$

The evolution equation for $\tilde{\mathcal{A}}_n$ is

$$\tilde{\mathcal{A}}_{nt} - g_n t\tilde{\mathcal{A}}_{ny} + 2i\alpha^2\Psi\cos(2\alpha y)\tilde{\mathcal{A}}_n = \frac{i\hbar_n}{2}\tilde{\mathcal{A}}_{nyy}, \tag{2.17}$$

where $g_n \equiv \beta\hbar_n$ is the effective gravity of mode n. By introducing a new independent variable,

$$\tilde{y} \equiv y + \tfrac{1}{2}g_n t^2, \tag{2.18}$$

we place (2.17) into the form,

$$\tilde{\mathcal{A}}_{nt} + 2i\alpha^2\Psi\cos\left[2\alpha\left(\tilde{y} - \frac{1}{2}g_n t^2\right)\right]\tilde{\mathcal{A}}_n = \frac{i\hbar_n}{2}\tilde{\mathcal{A}}_{n\tilde{y}\tilde{y}}. \tag{2.19}$$

The initial condition for (2.19) is $\tilde{\mathcal{A}}_n(\tilde{y}, 0) = -R_n^2\epsilon_n\sigma_n$.

On comparing (2.19) with (2.15) we see that the transformation has eliminated the nonperiodic coefficient y from the problem. In exchange for this simplification there is an unsteady potential in (2.19). However, this is a small price to pay because (2.19) can be solved numerically on the interval $0 < \tilde{y} < \pi$ using periodic boundary conditions. Because of the nonseparable y and t dependence of the exponential factor in (2.16) the solution in terms of the original variables is not periodic, and so (2.15) must be solved on an infinite domain. From a numerical perspective this would typically involve the imposition of conditions at some artificially specified domain boundaries, $y_{\min}$ and $y_{\max}$. By using (2.19), we avoid all these complications.

The decomposition in (2.16) shows that the local wave frequency changes with both latitude and time, as a result of the arrival of wave packets falling from higher latitudes. The temporal increase of the wave frequency may ultimately invalidate the NIO approximation.

3. Beta-dispersion

We begin by reviewing an extreme case in which there is no geostrophic flow ($\Psi = 0$) but $\beta \neq 0$. Then the solution of (2.19) is $\tilde{\mathcal{A}}_n(\tilde{y}, t) = -R_n^2\epsilon_n\sigma_n$ (this is essentially the solution of D'Asaro, 1989). We then reconstruct the solution by performing the sum in (2.6) (with an upper limit $n = 40$). The results are summarized in Figure 3.

Figures 3a and 3c show contours of constant 'speed,' $\sqrt{L\mathcal{A}L\mathcal{A}^*}$, and 'shear,'

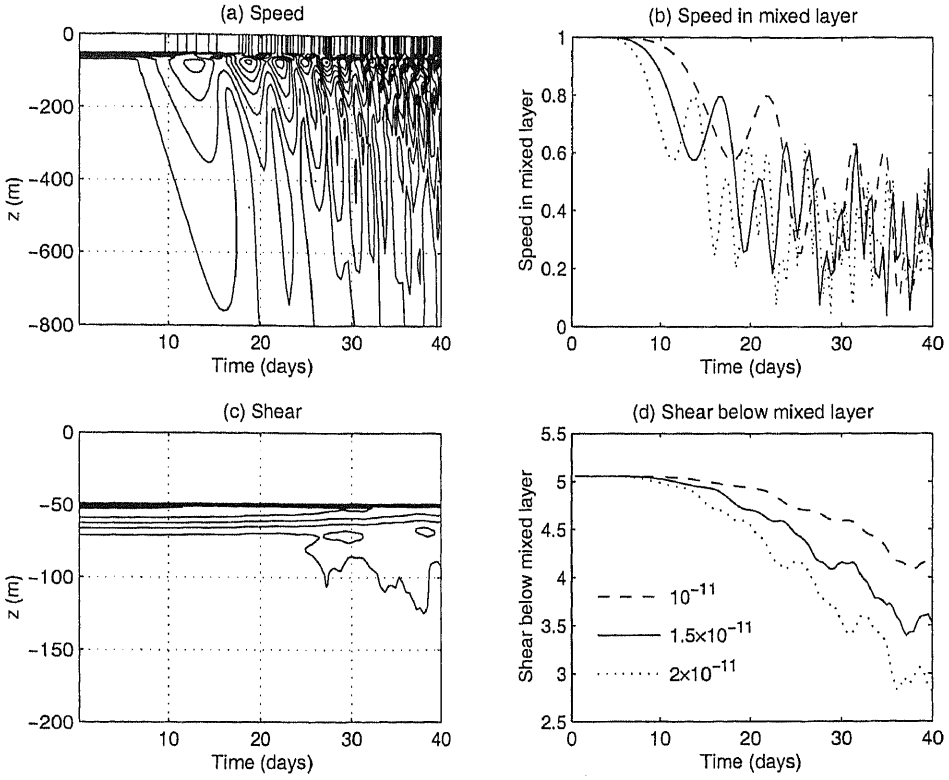

Figure 3. Evolution of the NIO fields on a β-plane with no geostrophic flow ($\Psi = 0$). Panels (a) and (c) show contours of constant speed and shear amplitude as a function of time and depth with $\beta = 1.5 \times 10^{-11}$ m^{-1} s^{-1}. Panel (b) displays the amplitude of the speed in the mixed layer as a function of time and panel (d) shows a similar picture for the shear amplitude at $z = -51$ m. In panels (b) and (d) we compare three different values of β: $\beta = 10^{-11}$, 1.5×10^{-11} and 2×10^{-11} in units of m^{-1} s^{-1}.

$\sqrt{L_z \mathcal{A} L_z \mathcal{A}^*_z}$, in the (z, t) plane[4] with $\beta = 1.5 \times 10^{-11}$ m^2 s^{-1}. The β-dispersion mechanism results in vertical transmission of speed but the shear remains localized at the base of the mixed layer for at least 40 days. As D'Asaro (1989) remarks, the difference is because β-dispersion operates most effectively on the low vertical modes which contain a substantial fraction of the energy, but a much smaller proportion of the shear. Figure 3b shows the evolution of speed in the mixed layer for three different values of β (the difference between the three cases is an obvious rescaling of time). The initial decay due to radiation damping is very slow but as t increases the factor $\exp[-i\hbar_n \beta^2 t^3/6]$ in (2.16) precipitates a sudden loss of modal coherence. This effect depends sensitively on β so that at high latitudes (small β) the decay of mixed-layer speed is delayed. Figure 3d shows that

4. With $\Psi = 0$ both the speed and the shear are independent of y. Thus, Figure 3 applies at all horizontal positions.

the shear immediately below the base of the mixed layer (at a depth of 51 m) decays by only 40% over 40 days.

In Figure 3b the initial monotonic decrease of the mixed layer speed is interrupted by the onset of 'bouncing.' As time progresses, the bounce frequency increases, while the amplitude varies irregularly. The bouncing energy level is a result of both the β-effect and the uniform initial amplitude of the NIOs: waves 'falling' from the north arrive with the relatively high frequency characteristic of those latitudes, and the attendant interference results in rapid fluctuations of energy level in the mixed layer. These fluctuations would be reduced by using an initial condition which is structured so that the energy decreases to the north.

The main point of this section is that β-dispersion alone is not sufficient to explain the total decay of near-inertial activity in the mixed layer in one or two weeks: β-dispersion operates effectively on the low vertical modes, but a substantial fraction of the energy (and most of the shear) is contained in the high vertical modes. Further, with no geostrophic vorticity, there is no horizontal modulation of the NIO energy density.

4. Beta-dispersion and geostrophic vorticity

We now turn to the combined effects of β-dispersion and geostrophic vorticity. We use the 'sinusoidal' geostrophic flow in (2.9) with the parameter values in Table 1. This is the 'standard case' used in paper I. We also use $\beta = 1.5 \times 10^{-11}$ m^{-1} s^{-1}; the nondimensional β-parameter defined in (2.11) is $\hat{\beta} = 0.96$.

The Schrödinger equation (2.19) is solved with 256 grid-points in the interval $0 < \eta \equiv \alpha y < \pi$ using the Crank-Nicholson scheme described by Garcia (1994). Figures 4 and 5 show a selection of low-order vertical modes plotted in the original stationary coordinate system. Figure 4, with $\beta = 0$, is a reprise of the results in paper I; the main point here is that there is a regular pattern of focussing then defocussing at the vorticity minima, with no asymmetry (in η) about the vorticity minimum at $\eta = \pi/2$. Figure 5 shows the effects of β; the low vertical modes, with larger values of $g_n = \beta f_0 R_n^2$, display strong accelerations toward the equator.

Figures 6 through 9 show the results of reconstituting the solution by summing over the 40 vertical modes. The main difficulty in visualizing the results is that when β and Ψ_0 are both nonzero the near-inertial fields are strongly dependent on both horizontal and vertical position.

Figure 6 shows the solution by plotting the speed, $|L\mathcal{A}| = \sqrt{u^2 + v^2}$, as a surface above the (η, z)-plane at four instants.[5] The radiation of the disturbance out of the mixed layer and into the deeper ocean is rapid so that at 20 days (Fig. 6b) there is a substantial amount of energy at 200 m and the kinetic energy density ($|L\mathcal{A}|^2/2$) at some points in the mixed layer has fallen to less than 10% of its initial value. However, because of the geostrophic vorticity, strong horizontal modulations of near-inertial energy density develop.

5. Figure 9 of paper I shows the equivalent of Figure 6, except with $\beta = 0$.

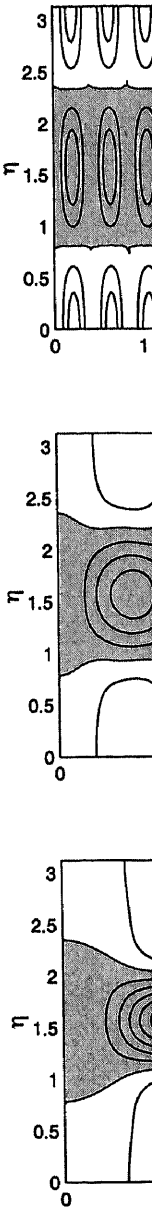

Figure 4. Evo
$\eta = \alpha y$, an
$\mathcal{A}_n = 1$ at
patterns are
and defocus
greater than

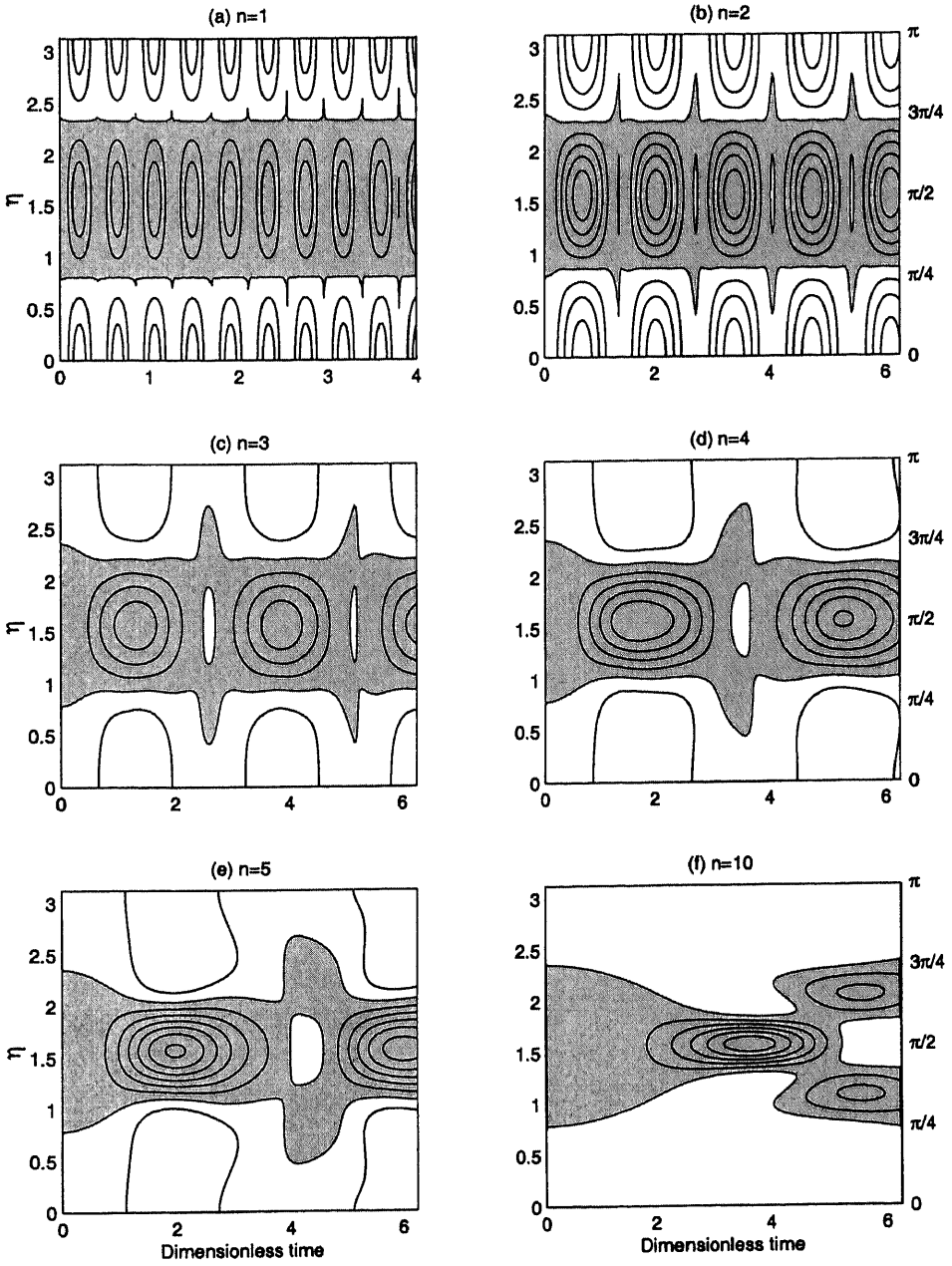

Figure 4. Evolution of the "energy density," $|\mathscr{A}_n|^2$, against the dimensionless horizontal coordinate, $\eta = \alpha y$, and time, t/T, with $\beta = 0$ and $\Psi = 4000\ \mathrm{m^2\,s^{-1}}$. The timescale T is $T \equiv 2/|\zeta_{\min}|$, and $\mathscr{A}_n = 1$ at $t = 0$. Shown are selected vertical modes: $n = 1, 2, 3, 4, 5$ and 10. With $\beta = 0$ the patterns are symmetric about the vorticity minimum at $\eta = \pi/2$; each mode alternately focusses and defocusses (like a seiche). The shading denotes the regions where the amplitude, $|\mathscr{A}_n|$, is greater than unity (that is, the uniform initial value).

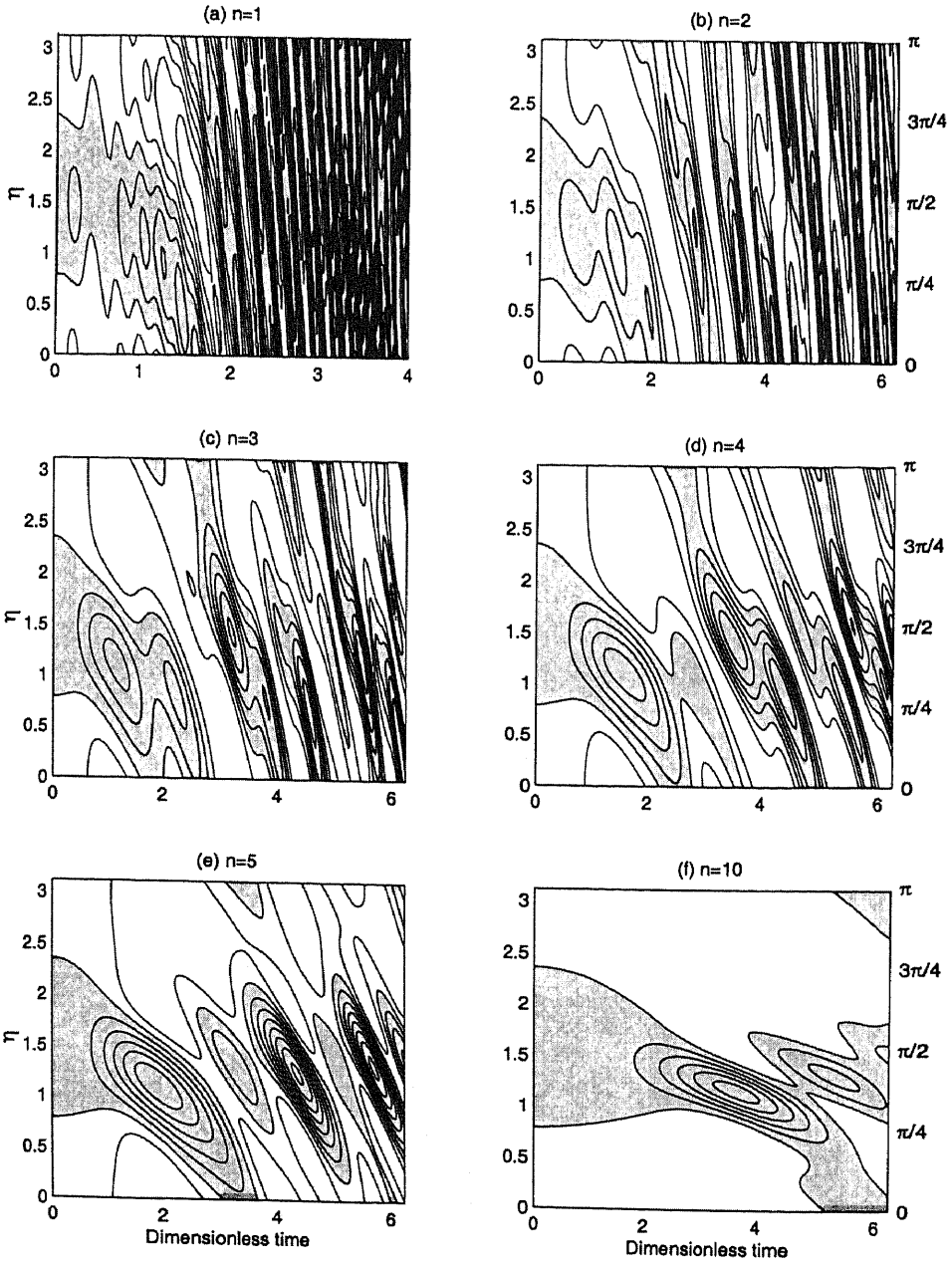

Figure 5. Evolution of the "energy density," $|\mathscr{A}_n|^2$, against the dimensionless horizontal coordinate, $\eta = \alpha y$, and time, t/T, with $\hat{\beta} = 0.96$ and $\Psi = 4000\ \mathrm{m^2\ s^{-1}}$. The timescale T is $T \equiv 2/|\zeta_{\min}|$, and $\mathscr{A}_n = 1$ at $t = 0$. Shown are selected vertical modes: $n = 1, 2, 3, 4, 5$ and 10. At first, the energy density is focussed into the minima of the $\beta y + (\zeta/2)$ potential. But, eventually, each mode tunnels through the potential barrier and 'falls' toward the equator. Both the time for focussing and the escape time are strong functions of the vertical mode number. The shading denotes the regions where the amplitude, $|\mathscr{A}_n|$, is greater than unity (that is, the uniform initial value).

In Figure 7 we display the speed, $|L\mathcal{A}| = \sqrt{u^2 + v^2}$, at the vorticity maximum, $\eta = 0$, and at the vorticity minimum, $\eta = \pi/2$, and we compare three cases:

(i) Geostrophic flow alone; $\hat{\beta} = 0$;

(ii) Geostrophic flow with $\hat{\beta} = 0.96$;

(iii) No geostrophic flow and $\beta = 1.5 \times 10^{-11}\ \mathrm{m^{-1}\ s^{-1}}$.

The effects of β are striking (compare the top two panels of Fig. 7 with the two middle panels). When $\beta = 0$ (Figs. 7a and 7b) the near-inertial energy 'piles-up' below the base of the mixed layer and there is little subsequent vertical propagation over 40 days. However, with $\hat{\beta} = 0.96$ (Figs. 7c and 7d), the submixed layer wave field develops both short vertical lengthscales and high frequency fluctuations and there is rapid vertical transmission of the disturbance. Figure 7e shows the case with $\Psi = 0$ and $\beta \neq 0$ for which there is no horizontal modulation of the near-inertial wavefield.

Another feature of the speed is displayed in Figure 8. This shows the back-rotated velocity components, $\exp(\mathrm{i}f_0 t)(u + \mathrm{i}v)$, at vorticity maximum ($\eta = 0$) and vorticity minimum ($\eta = \pi/2$) at depth $z = -80$ m. Panels (a) and (b) show the time series of the backrotated velocities for cases (i) and (ii); the β-shift causes the oscillation frequency to increase with time, as displayed by the exponential factor on the right of (2.16).[6] Panels (c) and (d) show hodographs of the back-rotated velocity components for cases (i) and (ii) above.

Based on panels (c) and (d) of Figure 8 we see that when $\beta = 0$, the back-rotated vector, $\exp(\mathrm{i}f_0 t)(u + \mathrm{i}v)$, rotates *counterclockwise* at vorticity minimum and *clockwise* at the vorticity maximum. The counterclockwise rotation at the vorticity minimum implies a shift out of the internal wave band, which is in agreement with Kunze's (1985) ray-tracing arguments. However, with $\beta \neq 0$, this rotation is completely dominated by the induced phase variation produced by the β-shift. Thus, in Figure 8, with $\beta \neq 0$, the backrotated vector rotates clockwise at both the vorticity maximum and the vorticity minimum (this is also true at the *potential* minimum, $\eta \approx 1.32$).

In Figure 9 we display the backrotated shear, $\exp(\mathrm{i}f_0 t)(u + \mathrm{i}v)_z$, at the same two positions as Figure 8 ($z = -80$ m and $\eta = 0$ and $\pi/2$). In shear, the effect of β is reduced because the β-effect chiefly influences lower-order vertical modes, but the shear is contained in higher-order vertical modes. However, the β-induced phase variation remains dominant, and this again leads to a clockwise rotation of the shear hodograph at vorticity minimum if $\beta \neq 0$ (again, this is anti-clockwise if $\beta = 0$).

Figure 10 shows the vertical penetration of the shear as a function of (η, z) at four times for case (ii). The initial focussing and subsequent vertical radiation of shear occurs near the minimum of the potential, V_n, at $\eta \approx 1.32$. Yet, relative to speed, the vertical penetration of shear is slow; at $t = 40$ days the shear is still mostly in the top 150 meters of the ocean. The

6. The increase in the frequency with time results from the propagation of wavepackets from higher latitudes toward the equator, and is a consequence of the uniform initial condition. If the initial condition was actually confined to a range in latitude, the frequency would not continue to increase indefinitely.

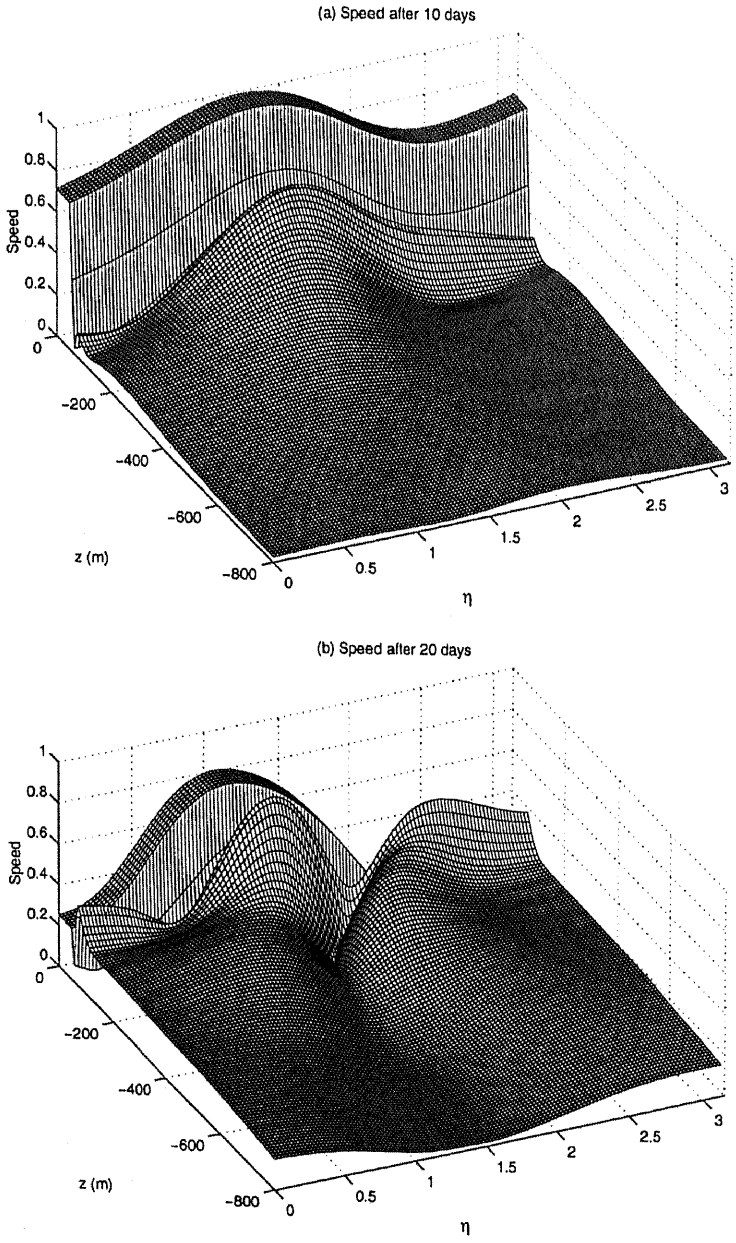

Figure 6. Snapshots of the speed, $\sqrt{|L\mathcal{A}|^2} = \sqrt{u^2 + v^2}$, as surface plots above the (η, z) plane at $t = 10$, 20, 30 and 40 days (panels (a)–(d)), for $-800\,\mathrm{m} \le z \le 0$ and $0 \le \eta \le \pi$. The mixed layer (with $H_{\mathrm{mix}} = 50$ m) is evident as the region with vertically uniform speed. The planetary vorticity gradient is $\beta = 1.5 \times 10^{-11}\ \mathrm{m^{-1}\,s^{-1}}$ and the geostrophic streamfunction is constructed using the parameter values in Table 1. At $t = 0$, the speed $\sqrt{|L\mathcal{A}|^2}$ is independent of η and equal to 1 in the mixed layer; in panel (a), after 10 days, the mixed-layer speed at the vorticity minimum ($\eta = \pi/2$) is amplified above its initial value. This amplification occurs because the low vertical modes in Figure 5 focus coherently near $\eta = \pi/2$.

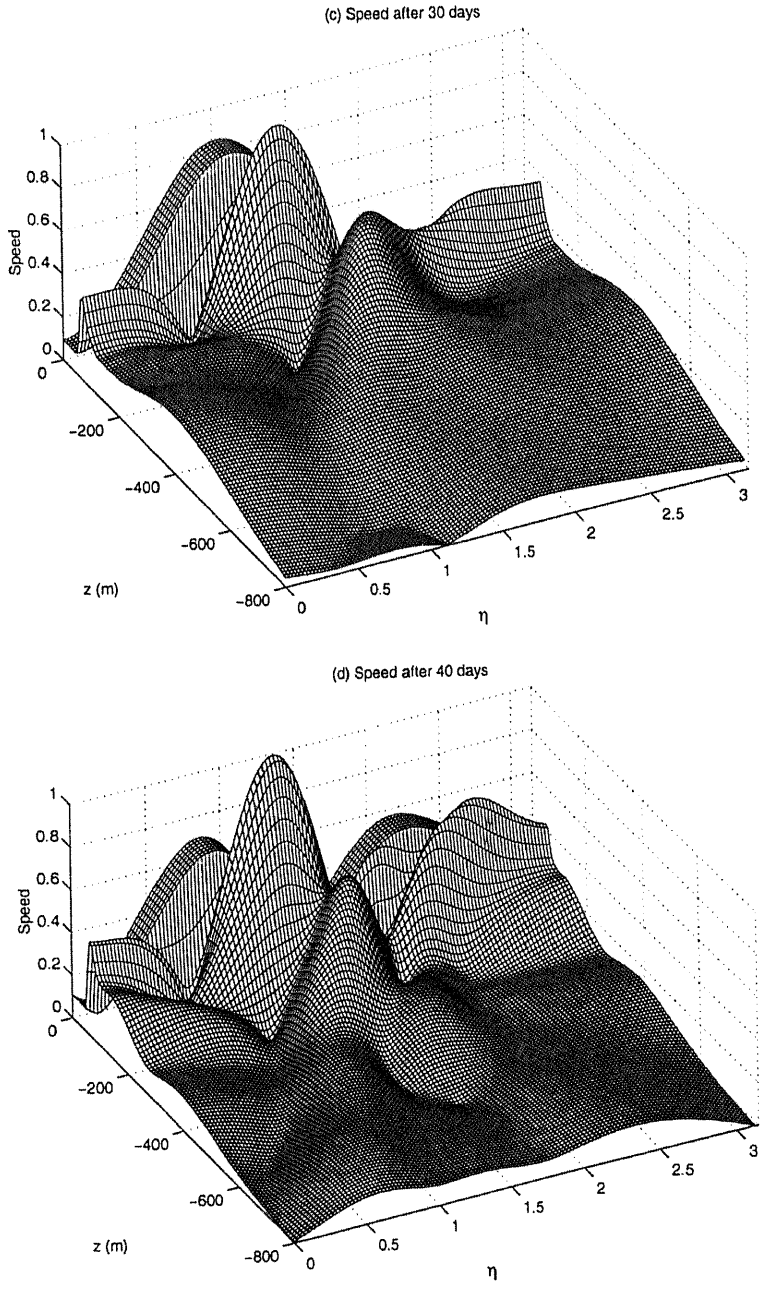

Figure 6. (Continued)

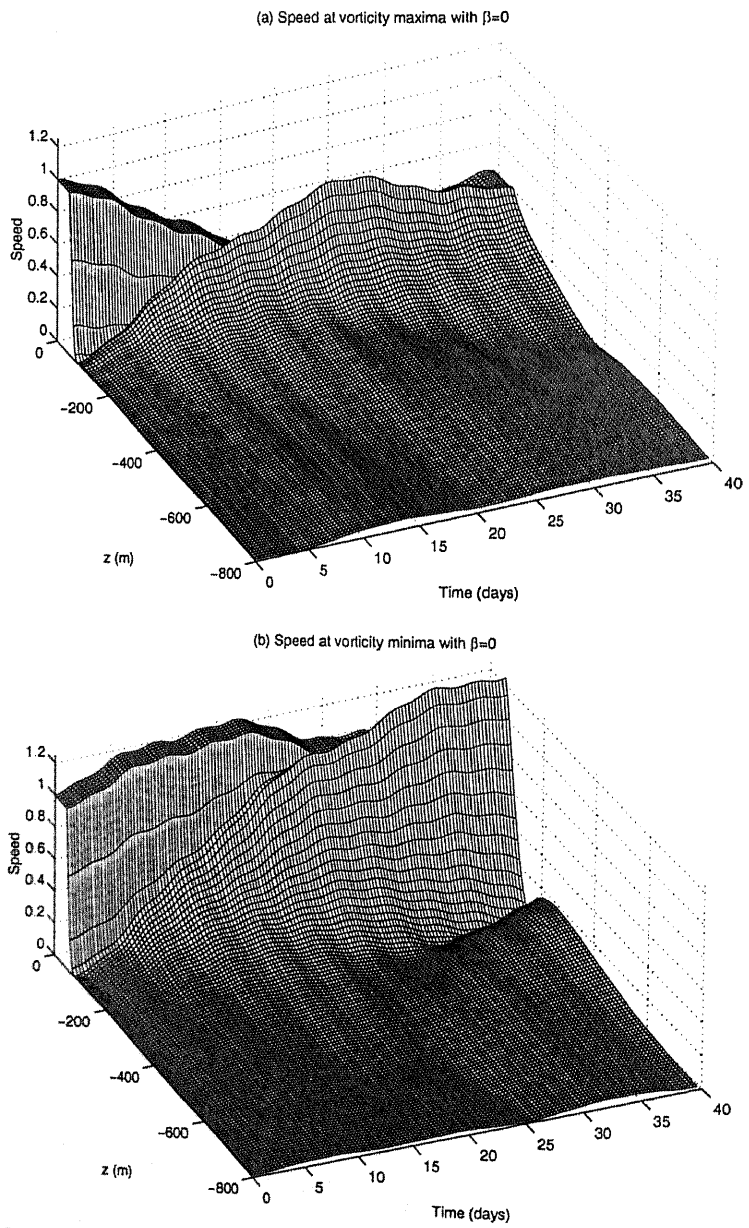

Figure 7. Variation of the speed, $\sqrt{|L.\mathscr{C}|^2} = \sqrt{u^2 + v^2}$, with and without geostrophic flow and the β-effect. Shown are surface plots of $|L.\mathscr{C}|$ above the (z, t) plane. Panels (a) and (b) show the solution with $\beta = 0$ and the geostrophic flow parameters of Table 1; (a) shows the evolution at vorticity maximum ($\eta = 0$) and (b) at vorticity minimum ($\eta = \pi/2$). Panels (c) and (d) show evolution for the case with $\hat{\beta} = 0.96$, at vorticity maximum and minimum, respectively. Panel (e) is the corresponding picture for $\Psi = 0$ and $\beta \neq 0$; in this final case the speed is horizontally uniform (that is, there is no distinction between vorticity maximum and vorticity minimum).

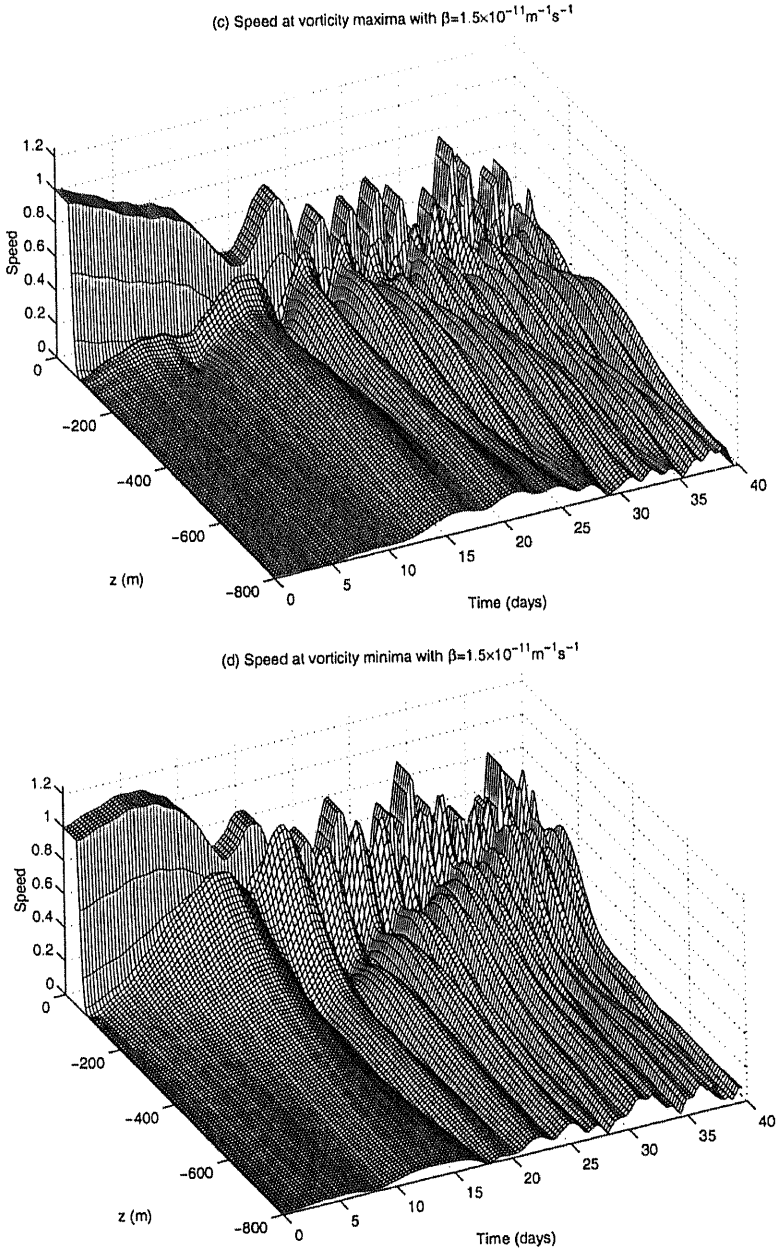

Figure 7. (Continued)

main feature in Figure 10 is the development of a submixed layer maximum in shear in the vicinity of the potential minimum. This feature also arises when $\beta = 0$, and was discussed in paper I; once again, we identify this enhancement in shear with the "beam" observed in the Ocean Storms experiment (D'Asaro *et al.*, 1995; D'Asaro, 1995a,b).

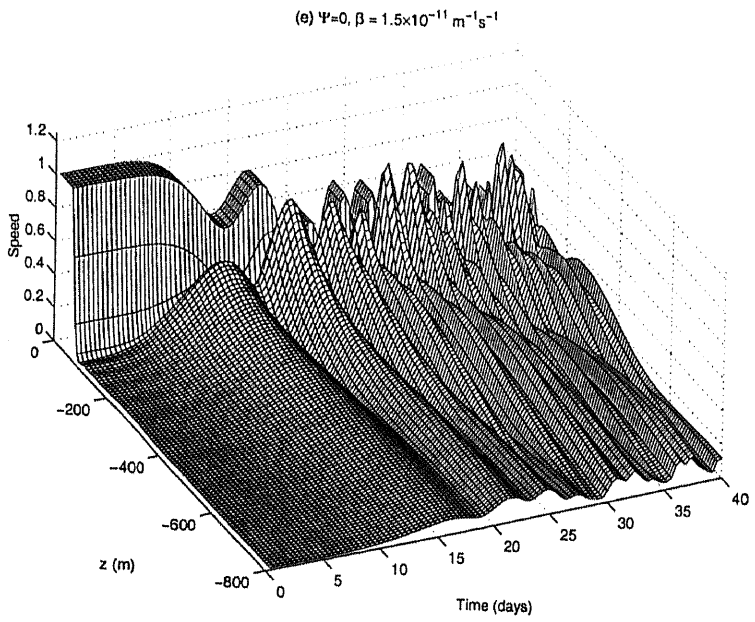

Figure 7. (Continued)

5. Strong dispersion

The numerical calculations reported above require the solution of the Shrödinger equation (2.7) for each vertical mode. This effort is time-consuming, and so it is worthwhile to explore further simplifications of the problem. One such simplification is the strong dispersion approximation (SDA) of Young and Ben Jelloul (1997). In this section we make a comparison between the SDA and the complete solution.

The SDA uses the spatially averaged field,

$$\bar{\mathscr{A}}(y, z, t) = \frac{\alpha}{\pi} \int_{y-\pi/2\alpha}^{y+\pi/2\alpha} \mathscr{A}(y', z, t)\, dy', \tag{5.1}$$

as the master variable. (The wavenumber of the sinusoidal shear flow is 2α so that the horizontal wavelength is π/α.) Then, provided that $\Psi/f_0 R_n^2$ is small, the result of spatially averaging (2.3) over the sinusoidal spatial scales is

$$L\bar{\mathscr{A}}_t + i\beta y L\bar{\mathscr{A}} + \frac{if_0}{2}\nabla^2\bar{\mathscr{A}} + \frac{iK}{f_0}L^2\bar{\mathscr{A}} = 0 \tag{5.2}$$

(Young and Ben Jelloul, 1997), where $K \equiv \alpha^2\Psi_0^2$ is the spatially averaged kinetic energy density of the sinusoidal flow in (2.9). The final term on the left-hand side of (5.2) is the rectified effect of the sinusoidal vorticity on the spatially averaged NIO fields.

The solution of (5.2), with the initial condition shown in Figure 2, is

$$L\bar{\mathscr{A}} = \sum_{n=1}^{40} \sigma_n \epsilon_n \hat{p}_n(z) \exp\left[-i\beta y t - \frac{i\hbar_n}{6}\beta^2 t^3 + \frac{iK}{\hbar_n} t\right]. \tag{5.3}$$

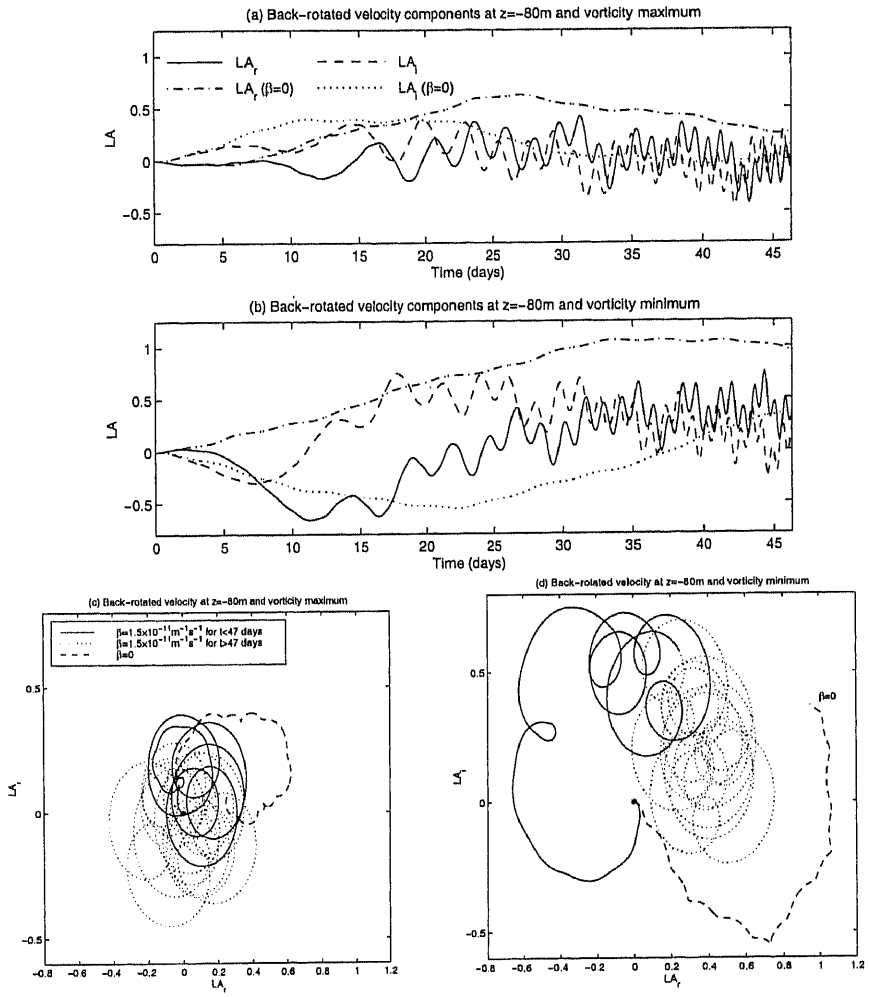

Figure 8. Back-rotated velocity, $L(\mathscr{A}_r + \mathrm{i}\mathscr{A}_i) = \exp(\mathrm{i}f_0 t)(u + \mathrm{i}v)$, at $z = -80$ m and vorticity maximum (panels (a) and (c)) and vorticity minimum (panels (b) and (d)). Panels (a) and (b) show time series of the back-rotated components with $\hat{\beta} = 0$ and $\hat{\beta} = 0.96$. Panels (c) and (d) show the rotation of the hodograph vector $L(\mathscr{A}_r + \mathrm{i}\mathscr{A}_i)$; the solid curve is the case with $\hat{\beta} = 0.96$ for $t < 30$ days, and is continued up to $t =$ 47 days by the dotted curve. The clockwise looping accelerates because of the $\beta^2 t^3$ factor in (2.16). The dashed curve is the case with $\hat{\beta} = 0$ which has much slower hodograph rotation; notice the different sense of rotation in panel (c) (clockwise) versus panel (d) (counterclockwise).

Unfortunately, the SDA fails for high vertical modes[7] so that there is no justification for including the large-n terms in (5.3). We press on, and address this criticism by making a comparison between the simple approximation in (5.3) with the full numerical solution.

7. As n increases, R_n decreases so that $\Psi/f_0 R_n^2$ is not small for high vertical modes.

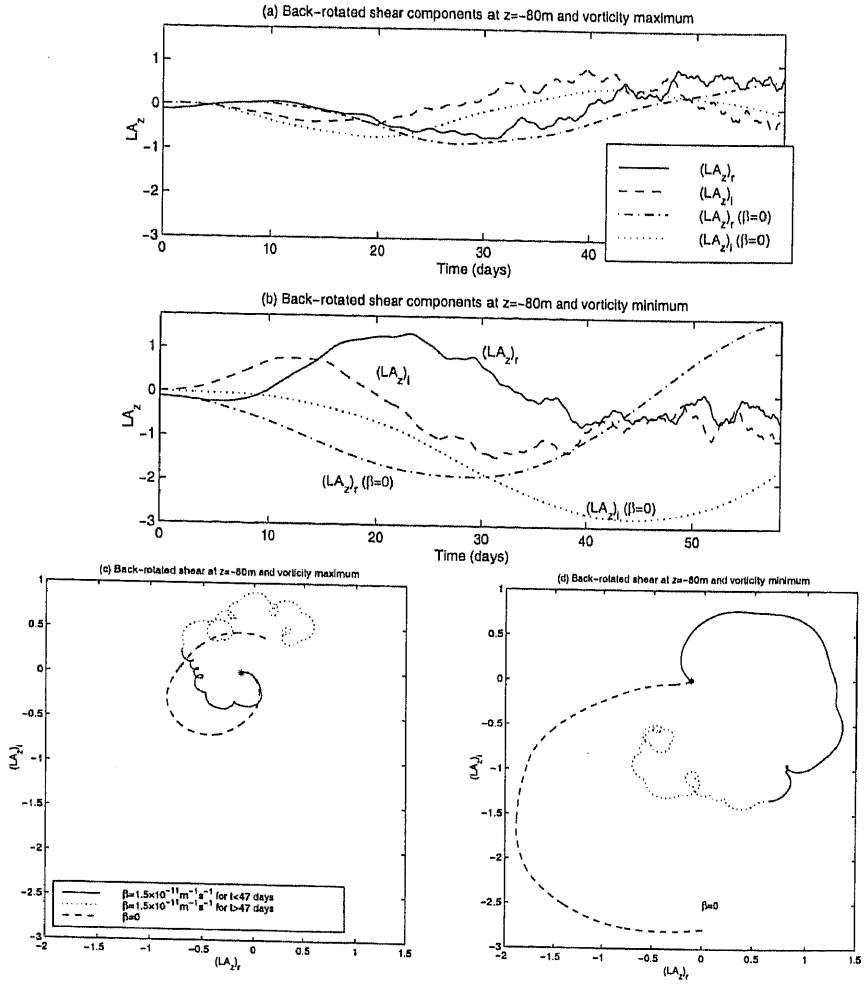

Figure 9. Back-rotated shear, $L(\mathscr{A}_r + \mathrm{i}\mathscr{A}_i)_z = \exp(\mathrm{i}f_0 t)(u + \mathrm{i}v)_z$, at $z = -80$ m and vorticity maximum (panels (a) and (c)) and vorticity minimum (panels (b) and (d)). Panels (a) and (b) show time series of the back-rotated components with $\hat{\beta} = 0$ and $\hat{\beta} = 0.96$. Panels (c) and (d) show the rotation of the shear hodograph vector $L(\mathscr{A}_r + \mathrm{i}\mathscr{A}_i)_z$. In panels (c) and (d), the solid curve shows the case with $\hat{\beta} = 0.96$ for $t < 30$ days, and is continued up to $t = 47$ days by the dotted curve. The dashed curves show the case with $\hat{\beta} = 0$; notice the different sense of rotation in panel (c) (clockwise) versus panel (d) (counterclockwise).

From the full numerical solution we may construct an 'exact' analog to (5.3). This is the horizontal average,

$$L\bar{\mathscr{A}} = \bar{u} + \mathrm{i}\bar{v} \equiv \frac{\alpha}{\pi}\int_0^{\pi/\alpha} (u + \mathrm{i}v)\, \mathrm{d}y. \tag{5.4}$$

In Figure 11a we compare the speed computed from (5.3) with the speed average, $|\bar{u} + \mathrm{i}\bar{v}|$ from (5.4). (Notice $|\bar{u} + \mathrm{i}\bar{v}|$ is independent of y.) The strong dispersion approximation gives a good prediction of the decay of the speed average over the first ten or twelve days.

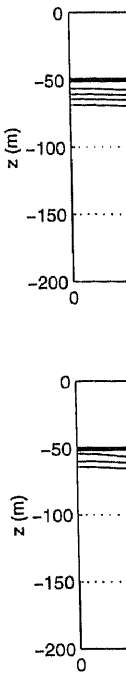

Figure 10. Snap
geostrophic f
-800 m $\leq z$
Figure 2b. Th
layer into the
vertical dash
this vorticity

In a similar
$|\bar{u}_z + \mathrm{i}\bar{v}_z|$, and
from (5.3). In
-51 m. Unfo
it poorly appr

To summa
vertical mode
energy, SDA
layer.

6. Conclusio

The transi
interior is ob

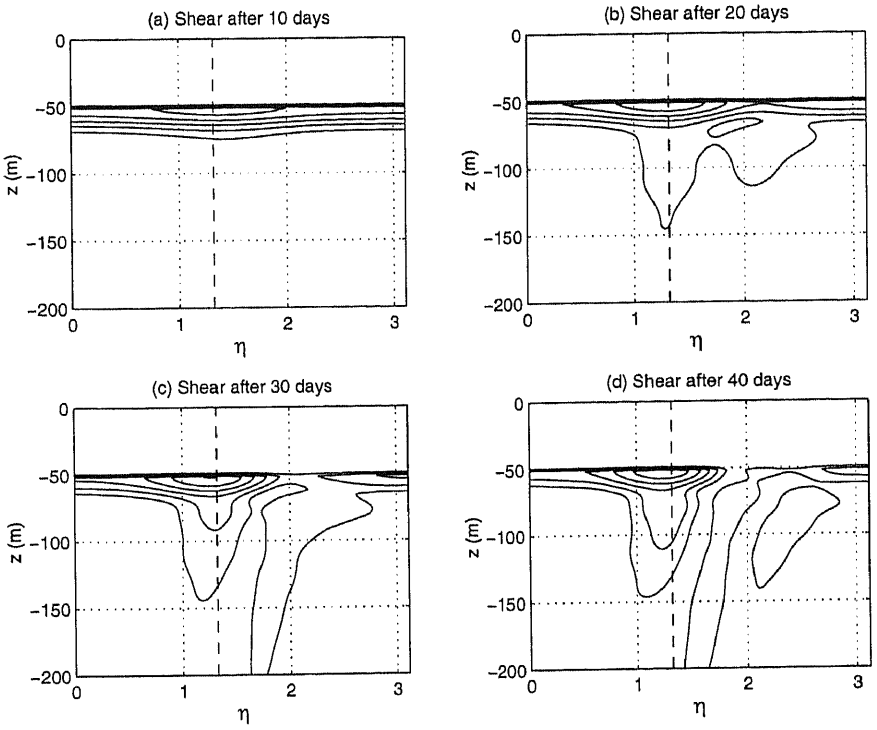

Figure 10. Snapshots of the distribution of shear amplitude, $\sqrt{u_z^2 + v_z^2}$, in the case with $\hat{\beta} = 0.96$ and geostrophic flow parameters in Table 1, at times $t = 10$, 20, 30 and 40 days (panels (a)–(d)), for $-800\text{ m} \le z \le 0$ and $0 \le \eta \le \pi$. The contour interval in all panels is 1 in the same units as Figure 2b. The main effect of the geostrophic vorticity is to focus the shear at the base of the mixed layer into the neighborhood of the potential minimum at $\eta \approx 1.32$; this location is shown by the vertical dashed lines. The vertical radiation of the shear then occurs mostly in the neighborhood of this vorticity minimum.

In a similar way, we may construct the shear average from the full numerical solution, $|\overline{u}_z + \mathrm{i}\overline{v}_z|$, and compare it to the shear in strong dispersion approximation, $|L\mathscr{U}_z|$ calculated from (5.3). In Figure 11b we show the comparison at the base of the mixed layer, $z = -51$ m. Unfortunately, the SDA inaccurately predicts a very rapid decay, primarily because it poorly approximates the high-order modes in which most of the shear resides.

To summarize: the SDA is accurate for low vertical modes and inaccurate for high vertical modes. Consequently, while the SDA reliably predicts the decay of mixed-layer energy, SDA fails to represent the much slower decay of the shear at the base of the mixed layer.

6. Conclusions

The transmission of near-inertial oscillations from the mixed layer into the ocean's interior is observed to occur on a timescale of between ten and twenty days. We have

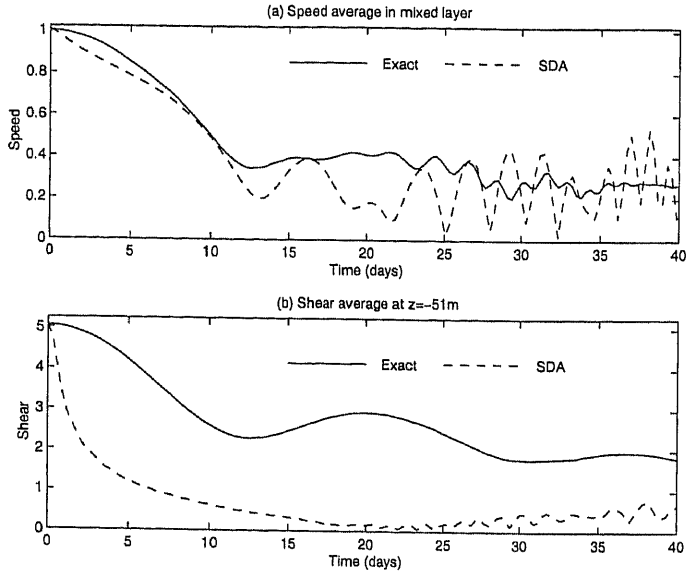

Figure 11. A comparison of the SDA in (5.3) with the 'exact' result obtained by numerical solution. (a) A comparison of the average speed in the mixed layer; the SDA provides a reliable estimate of the decay of speed over the first 12 days. (b) A comparison of the shear average immediately below base of the mixed layer. Because it seriously misrepresents the evolution of high vertical modes, the SDA grossly overestimates the rate of decay of shear.

shown in this paper that this relatively fast decay can be explained using a combination of a background geostrophic flow and the β-effect (even without the additional tuning of parameters suggested in paper I).

We emphasize that this rapid decay of NIO energy and shear requires *both* geostrophic flow and the β-effect. The two processes acting in concert are much more effective than either acting alone. Roughly speaking, β affects one part of the NIO wave spectrum, and the geostrophic flow a different part. The dephasing of the *low* vertical modes is accelerated by β, whereas the geostrophic flow has a stronger effect on the *high* vertical modes.

Note that the nondimensional parameter, $\hat{\beta}$, given in (2.11b), is crucial to this concerted effect. This parameter is the ratio of β to the geostrophic vorticity gradient. Therefore, it varies with both the latitude and with the model of the local eddy field. The computations reported in Section 4 all use $\hat{\beta} = 0.96$. But, we may increase α whilst holding $\alpha\Psi$ constant. Thus, we fix the kinetic energy density but decrease $\hat{\beta}$. Computations of this kind with $\hat{\beta} = 0.24$ ($\alpha^{-1} = 40$ km) produce solutions much like the cases reported in paper I (with $\beta = 0$). This suggests that the combination of β and a more complex velocity field, with a mixture of spatial scales, may be qualitatively different.

In addition to rapid decay of the mixed-layer NIOs, the model shows that the wavefield develops vertical and horizontal inhomogeneities. The horizontal modulations are solely a result of the geostrophic vorticity. That is, with $\Psi = 0$ and $\beta \neq 0$, the NIO energy density is

horizontally homogeneous (just as in the initial condition). The spatial inhomogeneities which result if $\Psi \neq 0$ can be strong and our statement above that the mixed-layer NIOs decay rapidly requires qualification: it is the spatially averaged (over a period of the sinusoidal shear flow) mixed-layer NIOs which decay rapidly. At some horizontal positions, persistent concentrations of NIO energy remain in the mixed layer. Moreover, for short times, and at certain locations, the mixed-layer NIO energy density can increase above initial levels.

The patterns of near-inertial energy and shear are complicated functions of both depth and horizontal position. Broadly speaking, enhanced near-inertial energy levels are correlated with environmental features, such as geostrophic vorticity maxima or minima. More specifically, energy and shear build up beneath the minima of the effective 'potential,' $\beta y + \zeta/2$ (Kunze 1985). This provides an explanation of the "beam" in the Ocean Storms experiment (D'Asaro *et al.*, 1995; D'Asaro, 1995a,b).

This is, of course, a favorable comparison of an oversimplified model with inadequate observations; we cannot claim that everything is understood here. But the model in this paper contains a minimal set of ingredients and predicts a rapid propagation of near-inertial waves out of the mixed layer. The associated decay of the near-inertial activity in the mixed layer is best described as *radiation damping*.

Finally, we remark that our calculations do not offer support for Gill's (1985) viscous ($\nu\nabla^2\mathbf{u}$) parameterization of the decay process. Nor is a Rayleigh drag ($-\nu\mathbf{u}$) parameterization suggested. Instead a curious alternative is indicated by the strong dispersion approximation. Returning to the primitive equations, we can obtain the approximation in (5.3) by using:

$$u_t - (f_0 + \beta y)v + p_x = (K/f_0)Lv, \qquad v_t + (f_0 + \beta y)u - p_y = -(K/f_0)Lu, \tag{6.1}$$

where L is the differential operator defined in (2.2) and $K = \alpha^2\Psi^2$ is the kinetic energy density of the geostrophic flow. In terms of the complex velocity $u + \mathrm{i}v$, the unfamiliar terms on the right-hand side of (6.1) are:

$$(u + \mathrm{i}v)_t + \mathrm{i}(f_0 + \beta y)(u + \mathrm{i}v) + (p_x - \mathrm{i}p_y) = -(\mathrm{i}K/f_0)L(u + \mathrm{i}v). \tag{6.2}$$

The parameterization above is equivalent to adding an *imaginary* vertical viscosity, $\mathrm{i}f_0KN^{-2}$, to the primitive equations. This is unusual, but it is less *ad hoc* than either viscous or Rayleigh drag parameterizations: the imaginary viscosity is a physically motivated representation of the vertical radiative processes which carry near-inertial energy out of the mixed layer and into the deeper ocean.

However, as we have indicated in our discussion of Figure 11, the parameterization in (6.1) and (6.2) is reliable only for the low vertical modes. Consequently, while the decay of energy in the mixed layer is adequately represented, the parameterization seriously overestimates the rate at which the shear at the base of the mixed layer decays. For the same reason, the parameterization will move the shear downward into the deeper ocean far too quickly. For many purposes (e.g., mixing parameterizations based on Richardson

number) the vertical distribution of shear is more important than the distribution of speed. Thus, this failure of (6.2) is serious and we still lack a simple parameterization which reliably predicts the evolution of both speed and shear.

Acknowledgments. This research was supported by the National Science Foundation (Grant OCE-9616017). We thank Dan Rudnick for advice, comments and error detection, and Eric D'Asaro for useful discussions.

REFERENCES

Balmforth, N. J., S. G. Llewellyn Smith and W. R. Young. 1998. Enhanced dispersion of near-inertial waves in an idealized geostrophic flow. J. Mar. Res., *56,* 1–40.

D'Asaro, E. A. 1989. The decay of wind forced mixed layer inertial oscillations due to the β-effect. J. Geophys. Res., *94,* 2045–2056.

—— 1995a. Upper-ocean inertial currents forced by a strong storm. Part II: Modeling. J. Phys. Oceanogr., *25,* 2937–2952.

—— 1995b. Upper-ocean inertial currents forced by a strong storm. Part III: Interaction of inertial currents and mesoscale eddies. J. Phys. Oceanogr., *25,* 2953–2958.

D'Asaro, E. A., C. C. Eriksen, M. D. Levine, P. P. Niiler, C. A. Paulson and P. van Meurs. 1995. Upper-ocean inertial currents forced by a strong storm. Part I: Data and comparisons with linear theory. J. Phys. Oceanogr., *25,* 2909–2936.

Garcia, A. L. 1994. Numerical Methods for Physicists, Prentice-Hall, 368 pp + xiii.

Gill, A. E. 1984. On the behavior of internal waves in the wakes of storms. J. Phys. Oceanogr., *14,* 1129–1151.

Kunze, E. 1985. Near-inertial wave propagation in geostrophic shear. J. Phys. Oceanogr., *15,* 544–565.

Young, W. R. and M. Ben Jelloul. 1997. Propagation of near-inertial oscillations through a geostrophic flow. J. Mar. Res., *55,* 735–766.

Zervakis, V. and M. Levine. 1995. Near-inertial energy propagation from the mixed layer: theoretical considerations. J. Phys. Oceanogr., *25,* 2872–2889.

Received: *5 May 1998;* revised: *15 May, 1999.*